

Comparison of Internal Voltage Vectors of DFIG-based Wind Turbine Generator and Synchronous Generator during Asymmetrical Fault

Yuanzhu Chang, Ilhan Kocar, Jiabing Hu, Maxime Berger

Abstract--Fault signatures of doubly fed induction generator (DFIG) based wind turbine generators (WTGs) are different and more complex than that of synchronous generators (SGs). This paper proposes a new approach to elaborate the formation of the fault signatures of DFIG-based WTGs under asymmetrical faults and various fault ride through control. The proposed internal voltage vectors and equivalent circuit enable reorganizing the control schemes, electric and magnetic circuits of DFIG in terms of transient, positive- and negative-sequence components. This way, the characteristics of DFIG-based WTGs and SGs can be compared in a similar frame through their internal voltage vectors. The differences and similarities are summarized in support of protection and control designs.

Keywords: Asymmetrical fault, doubly fed induction generator (DFIG), fault ride through, short circuit, synchronous generator.

I. INTRODUCTION

DOUBLY fed induction generator (DFIG) based wind turbine generators (WTGs), also referred to as Type-III WTGs, have already become a standard asset like synchronous generators (SGs) in modern power systems. During faults on the grid side, DFIG-based WTGs have a complex behavior that is different from synchronous generators (SGs) [1]-[2]. The underlying reason is that DFIG-based WTGs employ fully controlled but partially sized converters which have limited current and voltage capabilities. These unconventional fault signatures yield new challenges for fault and protective relaying studies [3]-[8].

There is a number of research studies on the fault response of DFIG-based WTGs. In terms of instantaneous values, electromagnetic transient (EMT) type models of DFIG-based WTGs, such as those implemented in MATLAB/Simulink [9], RTDS [10] and EMTP [11], are employed to reproduce the detailed fault response for power system studies. The short-circuit current of DFIG-based WTGs is compared with that of SGs in [1] and with those of other types of WTGs in [2] and [12]. To further quantify the current signature, analytical models and expressions are proposed for crowbar protection [13]-[15] and for the fault ride through control of the converters [16]-[18]. Phasor models are also proposed in [19]-[20] to quickly address potential maloperation of protection relays operating on fundamental frequency quantities.

These studies mainly focused on the fault current signatures of DFIG-based WTGs. This way, the DFIG-based WTG is considered as a black box controlled current source when analyzing the waveforms and the results. Since the fault current is naturally resulting from a complex interaction between the faulted power system and the DFIG converters, some characteristics of the typical fault signature of DFIG-based WTG still remain unexplained.

From a historical perspective, the basic understanding and simplifications of SG in electromechanical and electromagnetic studies are based on the knowledge of its internal voltage (also known as electromotive force or EMF) [21]. A SG can be modeled from its armature side as a series of Thevenin's equivalent circuits consisting of sub-transient, transient and steady-state voltages and reactances [22]. Therefore, the classical fault analysis for SG-dominated power systems can be transformed into a circuit problem, which greatly facilitates the design and setting of protection systems [23]. This paper proposes representing the DFIG and its control schemes as seen from the stator side, using a similar approach to SGs, so that the fault response can be analyzed using a perspective that is familiar to power system engineers.

The internal voltage vectors proposed in this paper break the complex structure of the original DFIG model and bridge the relationship between the rotor states of the DFIG and the stator circuit. The proposed equivalent circuits and block diagrams reveal how the internal states are changed and how the internal voltage vectors are formed by specific control schemes. By comparing the internal voltage vectors of DFIG-based WTG and SG under asymmetrical faults in various control configurations, fault signatures are analyzed to understand their differences and similarities which are useful for protection and control designs.

The following sections are organized as follows. The internal voltage vectors and a new equivalent circuit of DFIG are proposed in Section II. Then, in Section III, the asymmetrical fault ride through (AFRT) schemes are integrated in terms of transient, positive- and negative-sequence components. By comparing with the classical model of SG in Section IV, the input-output (open-loop) relationship and the close-loop responses of DFIG-based WTGs are analyzed.

Y. Chang and I. Kocar are with Department of Electrical Engineering, the Hong Kong Polytechnic University, Hong Kong SAR, China (e-mail: yuanzhu.chang@polyu.edu.hk; ilhan.kocar@polyu.edu.hk).

J. Hu is with the School of Electrical and Electronic Engineering, Huazhong University of Science and Technology, Wuhan, China (e-mail: j.hu@mail.hust.edu.cn).

M. Berger is with the Université du Québec à Rimouski (UQAR), Rimouski, QC G5L 3A1, Canada (e-mail: maxime_berger@uqar.ca)

II. INTERNAL VOLTAGE VECTORS OF THE DFIG

A. Electric and Magnetic Circuits of the DFIG

As shown in the schematic of the DFIG-based WTG in Fig. 1, the stator winding of the DFIG is connected to the WTG transformer, and the rotor winding is connected to rotor side converter (RSC). Since the WTG transformer is typically delta-connected, the zero-sequence components on the grid side are isolated, and the three-phase instantaneous values in the DFIG electrical circuit can be expressed with space vectors [24]. In the two-phase stationary reference frame (denoted by $\alpha\beta$) and the two-phase rotor reference frame (denoted by dqr), the equations of the stator and rotor electrical circuits are,

$$\mathbf{U}_s^{\alpha\beta} = R_s \mathbf{I}_s^{\alpha\beta} + \frac{d\boldsymbol{\psi}_s^{\alpha\beta}}{dt} \quad (1)$$

$$\mathbf{U}_r^{dqr} = R_r \mathbf{I}_r^{dqr} + \frac{d\boldsymbol{\psi}_r^{dqr}}{dt} \quad (2)$$

In this paper, space vectors are represented with bold type. For example, \mathbf{U} , \mathbf{I} and $\boldsymbol{\psi}$ stand for voltage, current and flux linkage vectors, respectively. The superscript indicates the reference frame in which the vector is observed. Subscripts s and r refer to the stator and rotor, respectively. R is resistance.

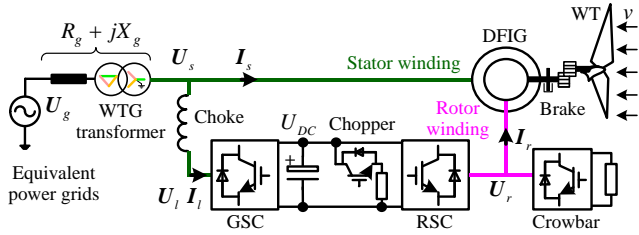


Fig. 1. Schematic of a DFIG-based WTG.

With the coordinate transformation from dqr to $\alpha\beta$, the rotor electrical circuit in (2) can be transformed as,

$$\mathbf{U}_r^{\alpha\beta} = R_r \mathbf{I}_r^{\alpha\beta} + \frac{d\boldsymbol{\psi}_r^{\alpha\beta}}{dt} - j\omega_r \boldsymbol{\psi}_r^{\alpha\beta} \quad (3)$$

where ω_r is the electrical angular frequency of the rotor.

The equations of DFIG magnetic circuit in the $\alpha\beta$ frame are,

$$\boldsymbol{\psi}_s^{\alpha\beta} = L_s \mathbf{I}_s^{\alpha\beta} + L_m \mathbf{I}_r^{\alpha\beta} \quad (4)$$

$$\boldsymbol{\psi}_r^{\alpha\beta} = L_m \mathbf{I}_s^{\alpha\beta} + L_r \mathbf{I}_r^{\alpha\beta} \quad (5)$$

where,

$$L_s = L_{l_s} + L_m \quad (6)$$

$$L_r = L_{l_r} + L_m \quad (7)$$

where L_s , L_r , L_m are the stator, rotor, and magnetizing inductances. L_{l_s} , L_{l_r} , are the stator and rotor linkage inductances.

The above equations of electrical and magnetic circuits of the DFIG correspond to the two-port network shown in Fig. 2.

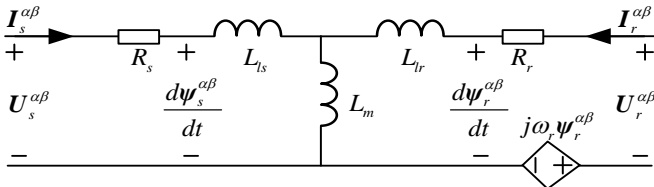


Fig. 2. Two-port network equivalent circuit of DFIG.

Due to the electromagnetic coupling and mechanical rotation between the stator and rotor windings, the relationship between

the stator voltage and stator current is determined by the rotor voltage, rotor current and rotor speed. This circuit is of a limited use for protection analysis due to the complexity involved in expressing the stator variables.

B. Definition of the Internal Voltage Vector

From a mathematical perspective, there are many choices for internal voltage vector to convert the above expressions into equivalent circuits. However, a helpful choice must directly reflect the internal states of DFIG and, more importantly, be independent of the stator variables.

In this paper, rotor flux linkage is selected to represent the internal state and the internal voltage vector \mathbf{E}_s is defined as the stator voltage generated by the rotor flux linkage.

First, the stator flux linkage can be replaced by rotor flux linkage and stator current as,

$$\boldsymbol{\psi}_s^{\alpha\beta} = \frac{L_m}{L_r} \boldsymbol{\psi}_r^{\alpha\beta} + \sigma L_s \mathbf{I}_s^{\alpha\beta} \quad (8)$$

where σ is the leakage factor of the DFIG, namely,

$$\sigma = 1 - \frac{L_m^2}{L_s L_r} \quad (9)$$

By substituting (8) into (1), the stator circuit can be transformed by,

$$\mathbf{U}_s^{\alpha\beta} = R_s \mathbf{I}_s^{\alpha\beta} + \sigma L_s \frac{d\mathbf{I}_s^{\alpha\beta}}{dt} + \mathbf{E}_s^{\alpha\beta} \quad (10)$$

where,

$$\mathbf{E}_s^{\alpha\beta} = \frac{L_m}{L_r} \frac{d\boldsymbol{\psi}_r^{\alpha\beta}}{dt} \quad (11)$$

Based on (10) and (11), a simple stator equivalent circuit of the DFIG is obtained as shown in Fig. 3. It indicates that the DFIG can be equivalent from its stator port as an internal voltage vector in series with R_s and σL_s . The internal voltage vector reflects the rotor flux linkage (internal state of DFIG) in the stator circuit. From this perspective, the stator current is a result of the voltage drop $\mathbf{U}_s - \mathbf{E}_s$ on the R_s and σL_s .

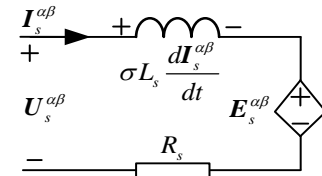


Fig. 3. Stator equivalent circuit of the DFIG in the time domain.

C. Internal Voltage based Equivalent Circuit

The rotor current in (2) can be replaced with the rotor flux linkage and stator current by,

$$\mathbf{I}_r^{dqr} = \frac{\boldsymbol{\psi}_r^{dqr}}{L_r} - \frac{L_m}{L_r} \mathbf{I}_s^{dqr} \quad (12)$$

By substituting (12) into (2), the rotor flux linkage becomes,

$$\frac{d\boldsymbol{\psi}_r^{dqr}}{dt} = \mathbf{U}_r^{dqr} + \frac{L_m}{\tau_r} \mathbf{I}_s^{dqr} - \frac{\boldsymbol{\psi}_r^{dqr}}{\tau_r} \quad (13)$$

where,

$$\tau_r = L_r / R_r \quad (14)$$

The electrical angular frequency of the rotor is changed by

the mechanical torque of the WT (T_m) and electromagnetic torque of the DFIG (T_{em}). This relationship can be described by

$$\frac{2H}{p\omega_1} \frac{d\omega_r}{dt} = T_m - T_{em} - K_D \frac{\omega_r}{p\omega_1} \quad (15)$$

where H and K_D is the inertia constant and damping factor of the DFIG rotor, respectively. p is the pole pairs. θ_r is the electrical rotor angle.

By transforming the differential equations in (13) and (15) with Laplace operator (s), the formation of the internal voltage vector can be described by the block diagram in Fig. 4.

Besides the armature reaction and electromagnetic induction of the DFIG, the rotor flux linkage is dominated by the rotor voltage. Considering the high inertia constant of the wind turbine, it is reasonable to neglect the rotor speed variation during the AFRT. The rotor voltage is governed by RSC control schemes and will be further analyzed in Section III in terms of the transient, positive- and negative-sequence components.

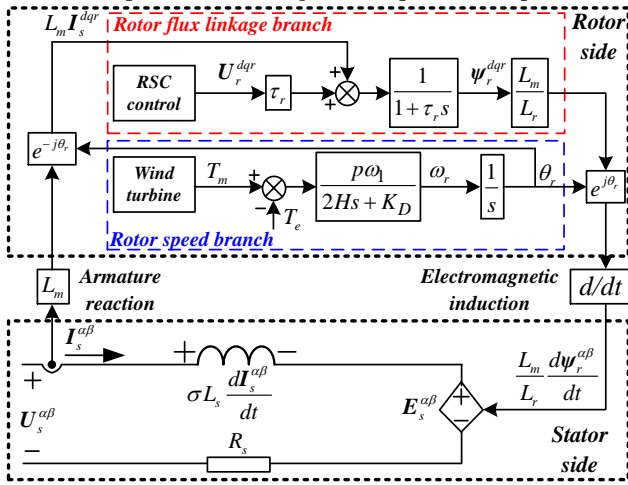


Fig. 4. Block diagram of the DFIG for forming the internal voltage vector.

III. INTERNAL VOLTAGE VECTOR AND CONTROL

A. Instantaneous Values and Components

During asymmetrical faults, the stator voltage is composed of positive- and negative-sequence components [25], and they can be written as a space vector in the $\alpha\beta$ frame as,

$$\mathbf{U}_s^{\alpha\beta} = \mathbf{u}_\alpha + j\mathbf{u}_\beta = \mathbf{U}_{s+}^{dq+} e^{j\omega_1 t} + \mathbf{U}_{s-}^{dq-} e^{-j\omega_1 t} \quad (16)$$

where ω_1 is the synchronous angular velocity. Superscripts $dq+$ and $dq-$ indicate two-phase synchronous reference frames rotating at ω_1 and $-\omega_1$, respectively. Subscripts $+$ and $-$ indicate positive- and negative-sequence components, respectively.

Although the stator voltage is suddenly changed by the faults, the existing rotor flux linkage cannot be altered abruptly [26]. As a result, a transient component (denoted by $'$) is induced and the rotor flux linkage vector is,

$$\boldsymbol{\psi}_r^{\alpha\beta} = \boldsymbol{\psi}_{r+}^{dq+} e^{j\omega_1 t} + \boldsymbol{\psi}_{r-}^{dq-} e^{-j\omega_1 t} + \boldsymbol{\psi}_r^{\prime\alpha\beta} \quad (17)$$

According to (11), the corresponding internal voltage vector is also composed of those three components as,

$$\mathbf{E}_s^{\alpha\beta} = \mathbf{E}_{s+}^{dq+} e^{j\omega_1 t} + \mathbf{E}_{s-}^{dq-} e^{-j\omega_1 t} + \mathbf{E}_s^{\prime\alpha\beta} \quad (18)$$

where,

$$\mathbf{E}_{s+}^{dq+} = j\omega_1 (L_m / L_r) \boldsymbol{\psi}_{r+}^{dq+} \quad (19)$$

$$\mathbf{E}_{s-}^{dq-} = -j\omega_1 (L_m / L_r) \boldsymbol{\psi}_{r-}^{dq-} \quad (20)$$

$$\mathbf{E}_s^{\prime\alpha\beta} = \frac{L_m}{L_r} \frac{d\boldsymbol{\psi}_r^{\prime\alpha\beta}}{dt} \quad (21)$$

B. Positive-sequence Internal Voltage and Model

During asymmetrical faults, the positive-sequence control of the RSC is designed to comply with the ‘‘positive-sequence reactive current’’ (IIR) injection requirement. The rotor current references are generated in the positive-sequence phase-locked loop (PLL) reference frame (denoted by $PLL+$) [27] as,

$$\mathbf{I}_{r+}^{PLL+\text{ref}} = -\frac{L_s}{L_m} K_{V+} (1 - U_{s+}) - \frac{U_{s+}}{\omega_1 L_m} \quad (22)$$

where K_{V+} is the IIR injection factor.

The rest of the current capacity of the RSC can be assigned to the ‘‘positive-sequence active current’’ (IIA). The positive-sequence rotor voltage generated by the inner-loop control is,

$$\mathbf{U}_{r+}^{PLL+} = R_r \mathbf{I}_{r+}^{PLL+} + j\omega_s \boldsymbol{\psi}_{r+}^{PLL+} + (K_{pi} + \frac{K_{ii}}{s})(\mathbf{I}_{r+}^{PLL+\text{ref}} - \mathbf{I}_{r+}^{PLL+}) \quad (23)$$

where K_{pi} and K_{ii} are the proportional and integral gains of the inner-loop controllers.

The terms multiplied by K_{ii} can be neglected because it is designed to remove the steady-state errors caused by the imperfect decoupling term [28] and has only a small contribution to the reference tracking [29]. The rotor voltage can be transformed into $dq+$ as,

$$\mathbf{U}_{r+}^{dq+} = (R_r - K_{pi}) \mathbf{I}_{r+}^{dq+} + j\omega_s \boldsymbol{\psi}_{r+}^{dq+} + K_{pi} \mathbf{I}_{r+}^{PLL+\text{ref}} e^{j\Delta\theta_{PLL}} \quad (24)$$

where $\Delta\theta_{PLL}$ and $\Delta\omega_{PLL}$ are the angle and angular velocity differences between $PLL+$ and the $dq+$, namely,

$$\Delta\theta_{PLL} = \theta_{PLL} - \omega_1 t = \int \omega_{PLL} dt - \omega_1 t = \int \Delta\omega_{PLL} dt \quad (25)$$

By substituting (24) into (13) and then replacing the rotor current with (12), the positive-sequence rotor flux linkage becomes,

$$\frac{d\boldsymbol{\psi}_{r+}^{dq+}}{dt} = -\frac{\boldsymbol{\psi}_{r+}^{dq+}}{\tau_{ri}} + \frac{L_m \mathbf{I}_{s+}^{dq+} + L_r \mathbf{I}_{r+}^{PLL+\text{ref}} e^{j\Delta\theta_{PLL}}}{\tau_{ri}} \quad (26)$$

where,

$$\tau_{ri} = L_r / K_{pi} \quad (27)$$

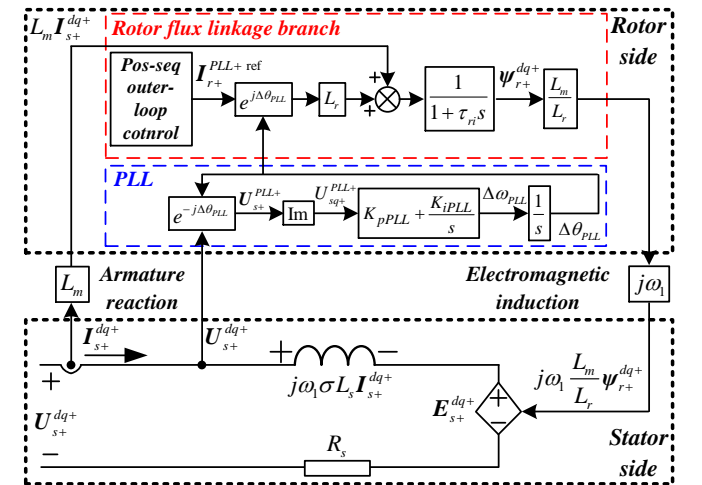


Fig. 5. Block diagram of DFIG-based WTG for forming the positive-sequence internal voltage vector.

With (26), the formation of the positive-sequence internal voltage vector is described by the block diagram in Fig. 5. K_{pPLL} and K_{iPLL} are the proportional and integral gains of the PLL.

Fig. 5 indicates that the positive-sequence internal voltage vector is formed by the rotor flux linkage branch and the PLL. The rotor flux linkage is altered, on one side, by the stator current through the armature reaction and, on the other side, by the rotor current references for the IIR and IIA injections.

C. Negative-sequence Internal Voltage and Model

The objective of the negative-sequence RSC control can be either balancing the stator current or complying with the “negative-sequence reactive current” (I2R) injection requirement of recent grid codes such as [30]. The negative-sequence rotor current references are generated in the PLL-frame as,

$$\mathbf{I}_{r-}^{PLL-ref} = j \left(\frac{1 - \omega_1 L_s K_{V-}}{\omega_1 L_m} \right) \mathbf{U}_{s-}^{PLL-} \quad (28)$$

where K_{V-} is the I2R injection factor.

By transforming (28) into $dq-$, the current references are,

$$\mathbf{I}_{r-}^{dq-ref} = j \left(\frac{1 - \omega_1 L_s K_{V-}}{\omega_1 L_m} \right) \mathbf{U}_{s-}^{dq-} \quad (29)$$

The negative-sequence rotor voltage generated by the inner-loop control is also simplified as,

$$\mathbf{U}_{r-}^{dq-} = (R_r - K_{pi}) \mathbf{I}_{r-}^{dq-} - j(\omega_1 + \omega_r) \boldsymbol{\psi}_{r-}^{dq-} + K_{pi} \mathbf{I}_{r-}^{dq-ref} \quad (30)$$

By substituting (30) into (13), the negative-sequence rotor flux linkage becomes,

$$\frac{d\boldsymbol{\psi}_{r-}^{dq-}}{dt} = -\frac{\boldsymbol{\psi}_{r-}^{dq-}}{\tau_{ri}} + \frac{L_r \mathbf{I}_{r-}^{dq-ref} + L_m \mathbf{I}_{s-}^{dq-}}{\tau_{ri}} \quad (31)$$

The formation of the negative-sequence internal voltage vector can be described with the block diagram in Fig. 6.

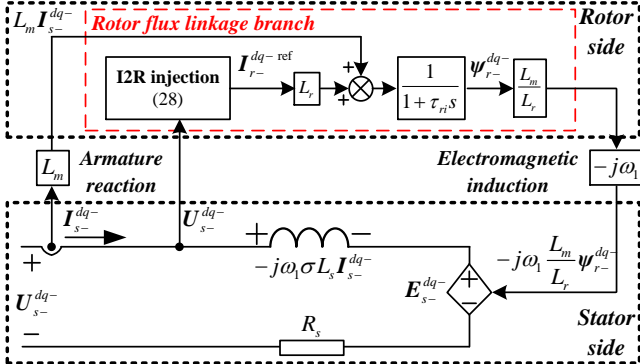


Fig. 6. Block diagram of DFIG-based WTG for forming the negative-sequence internal voltage vector.

Compared with the positive-sequence internal voltage vector in Fig. 5, the negative-sequence internal voltage vector in Fig. 6 is only determined by the rotor flux linkage branch with I2R injection, and the PLL is not involved.

D. Transient Internal Voltage and Model

During AFRT, the transient components are also adjusted by control schemes such as demagnetizing control [31] and inductance-emulating control [32]. If neglecting these transient components in the control design, these transient components will decay with a large time constant, which may also result in

over-modulation of the RSC.

Taking the inductance-emulating control as an example, the RSC mimics a constant inductance L_{RSC} for the transient components [32], and the transient rotor current is,

$$\mathbf{I}_r^{\prime\alpha\beta} = -\frac{L_m}{\sigma L_s L_r + L_s L_{RSC}} \boldsymbol{\psi}_s^{\prime\alpha\beta} \quad (32)$$

By substituting (8) into (32), the transient rotor flux linkage becomes,

$$\boldsymbol{\psi}_r^{\prime\alpha\beta} = \frac{1 - \sigma}{L_r + L_{RSC}} \frac{L_s L_r L_{RSC}}{L_m} \mathbf{I}_s^{\prime\alpha\beta} \quad (33)$$

According to (21), the transient internal voltage vector is,

$$\mathbf{E}_s^{\prime\alpha\beta} = \frac{L_m}{L_r} \frac{d\boldsymbol{\psi}_r^{\prime\alpha\beta}}{dt} = \frac{1 - \sigma}{L_r + L_{RSC}} L_s L_{RSC} \frac{d\mathbf{I}_s^{\prime\alpha\beta}}{dt} \quad (34)$$

The formation of the transient internal voltage vector can be described by the block diagram in Fig. 7.

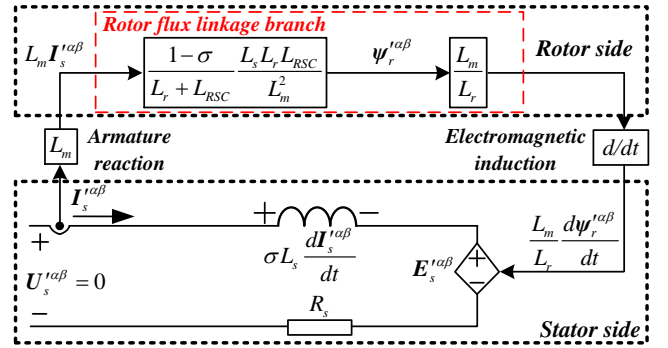


Fig. 7. Block diagram of DFIG-based WTG for forming the transient internal voltage vector.

According to (34), the transient internal voltage vector also emulates an inductance on the stator side, and the overall inductance seen from the stator port in the equivalent circuit is,

$$\frac{1 - \sigma}{L_r + L_{RSC}} L_s L_{RSC} + \sigma L_s = L_s \frac{\sigma L_r + L_{RSC}}{L_r + L_{RSC}} \quad (35)$$

IV. COMPARISON BETWEEN DFIG-BASED WTG AND SG ON INTERNAL VOLTAGE VECTORS

A. Internal Voltage and Equivalent Circuit of a SG

The classical model of a SG in [21] is adopted in this paper for the comparison. Unlike the full-order model of a SG in [33], the classical model simplifies the saliency effects in the sub-transient, transient and steady-state periods. It is reasonable because those saliency effects mainly contribute to the second harmonic components which are not the focus of this paper.

This SG model equipped with two field windings (fd and fq) and two damper windings (ld and lq), where fd is governed by the DC excitation voltage U_{fd} and fq is a short-circuited winding that has the same structure as fd . This way, $L''_d = L''_q$, $L'_d = L'_q$ and $L_d = L_q$. This SG model can be reorganized as (35) and Fig. 6 by using the inductance L''_d in the equivalent circuit. The SG model equations are as follows:

$$\mathbf{U}_s^{\alpha\beta} = R_s \mathbf{I}_s^{\alpha\beta} + L''_d \frac{d\mathbf{I}_s^{\alpha\beta}}{dt} + \mathbf{E}_s^{\alpha\beta} \quad (36)$$

$$\mathbf{E}_s^{\alpha\beta} = j\omega_1 \left(\frac{L''_{ad}}{L_{fd}} \boldsymbol{\psi}_{fd}^{dq} + \frac{L''_{aq}}{L_{fd}} \boldsymbol{\psi}_{fd}^{dq} \right) e^{j\theta} \quad (37)$$

$$\frac{d\psi_f^{dqr}}{dt} = -\frac{\psi_f^{dqr}}{\tau_f} + \frac{\sigma_f L_{ad}'' \mathbf{I}_s^{dqr}}{\tau_f} + \frac{\sigma_f L_{ad}'' \psi_f^{dqr}}{\tau_f L_{fd}} + U_{fd} \quad (38)$$

$$\frac{d\psi_l^{dqr}}{dt} = -\frac{\psi_l^{dqr}}{\tau_l} + \frac{\sigma_l L_{ad}'' \mathbf{I}_s^{dqr}}{\tau_l} + \frac{\sigma_l L_{ad}'' \psi_f^{dqr}}{\tau_l L_{fd}} \quad (39)$$

where,

$$\sigma_f = L_{fd} / (L_{fd} - L_{ad}'') \quad \sigma_l = L_{ld} / (L_{ld} - L_{ad}'') \quad (40)$$

$$L_{ad}'' = 1 / (1/L_{ad} + 1/L_{fd} + 1/L_{ld}) \quad (41)$$

$$\tau_f = \sigma_f L_{fd} / R_f \quad \tau_l = \sigma_l L_{ld} / R_l \quad (42)$$

L_{ad} is the mutual inductance. L_{fd} and L_{ld} are the leakage inductances of field and damper windings. τ_f and τ_l are the time constants of the field and damper windings. R_f and R_l are the resistances of the field and damper windings.

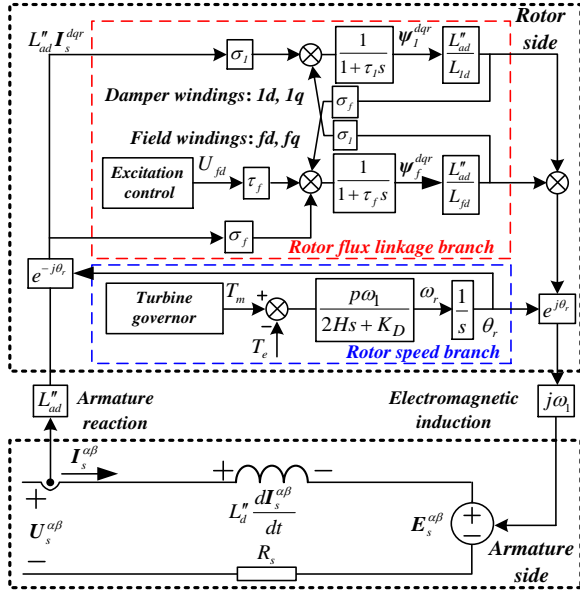


Fig. 8. Block diagram of SG for forming the internal voltage vector.

B. Comparison of the Internal Voltage Formation

By comparing (39) and (11) as well as Fig. 8 and Fig. 4, it is possible to conclude that the internal voltage vectors of SG and DFIG are both generated by the rotor flux linkage through the electromagnetic induction.

However, after integrating the AFRT control schemes into the equivalent circuit, the differences between SG and DFIG-based WTG can be seen. Since the DC excitation voltage is only applied to fd , only a positive-sequence internal voltage vector is induced in the SG. The magnitude of the internal voltage vector of the SG is governed by the rotor flux linkage branch, while the frequency and angle of the internal voltage are physically decided by the position and speed of the rotor. In contrast, due to the flexibility of the AC excitation, both the magnitude and frequency of the internal voltage vectors of the DFIG-based WTG are shaped by the rotor flux linkage branch. In addition to the positive-sequence internal voltage vector, negative-sequence and transient internal voltage vectors are generated by the DFIG AFRT control. It should also be noted that, considering the voltage and current control capabilities of the RSC, the transient, positive-sequence and negative-sequence control schemes may interfere with each other because they are coordinated with pre-defined priority to avoid

RSC overcurrent. This kind of coupling between positive- and negative-sequence systems only exist at the fault point in the classical fault analysis, which is not the case with a DFIG.

C. Comparisons of Internal Voltage Vector Responses

In the light of the similarity between the equivalent circuits of the DFIG-based WTG and SG, the internal voltage vectors are compared by EMT-type simulations using the 120 kV test system shown in Fig. 9. A DFIG-based wind park and a SG can be selected to connect to BUS1. The parameters of the DFIG-based WTG and SG are shown in Table I and Table II, respectively. Their internal voltage vectors are compared under a bolted double-line-to-ground short circuit applied at BUS3 at $t = 1$ s. The results are obtained with MATLAB/Simulink.

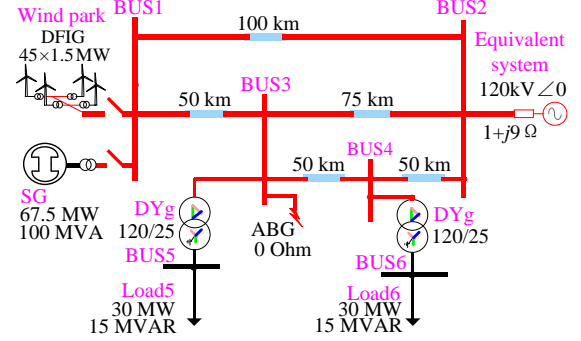


Fig. 9. Test system for the comparison of DFIG-based WTG and SG behavior.

TABLE I
PARAMETERS OF A 1.5 MW DFIG-BASED WTG

Parameter	Value	Parameter	Value
Stator voltage (LLRMS)	575 V	$\omega_1 L_s$	3.08 p.u.
Turns ratio (N_f/N_s)	3:1	$\omega_1 L_r$	3.06 p.u.
Rated active power	1.5 MW	$\omega_1 L_m$	2.9 p.u.
Power base	1.667 MVA	$\omega_1 L_{RSC}$	0.15 p.u.
R_s	0.023 p.u.	K_{pi}	2.4
R_r	0.016 p.u.	K_{ii}	128
ω_r	144 π rad/s	K_{pPLL}	180
ω_1	120 π rad/s	K_{iPLL}	1000
σ	0.1077	K_{V+}	2

TABLE II
PARAMETERS OF A 100 MVA SG

Parameter	Value	Parameter	Value
Stator voltage (LLRMS)	13.8 kV	$\omega_1 L_d$	1.880 p.u.
Power base	100 MVA	$\omega_1 L_{fd}$	0.236 p.u.
p	2	$\omega_1 L_{ld}$	0.243 p.u.
R_s	0.023 p.u.	$\omega_1 L_{ad}$	1.660 p.u.
R_f	0.0006 p.u.	$\omega_1 L_{ad}'$	0.112 p.u.
R_{ld}	0.0284 p.u.	$\omega_1 L_{ad}''$	0.332 p.u.
H	3.525 s	K_D	0.5

First, the internal voltage of SG is shown in Fig. 10. It can be seen that, during the asymmetrical fault, only positive-sequence internal voltage exists in the SG, and its magnitude smoothly changed in the sub-transient and transient periods.

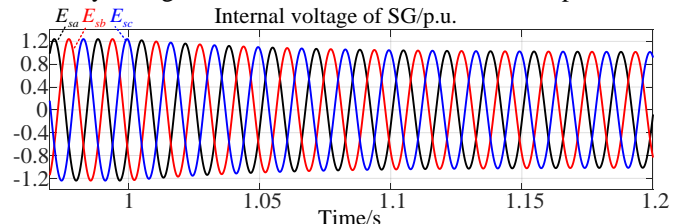


Fig. 10. Three-phase internal voltage of SG.

Second, the internal voltage of DFIG-based WTG, when K_V is 0, is shown in Fig. 11. By using the proposed models in Fig. 5, Fig. 6 and Fig. 7, the positive-sequence, negative-sequence, and transient components are obtained as Fig. 12.

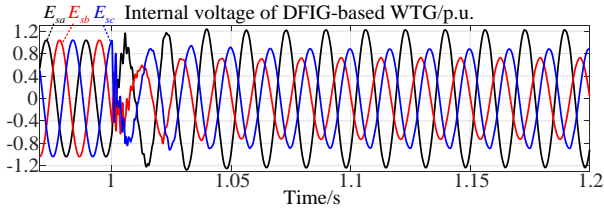


Fig. 11. Three-phase internal voltage of DFIG-based WTG when $K_V=0$.

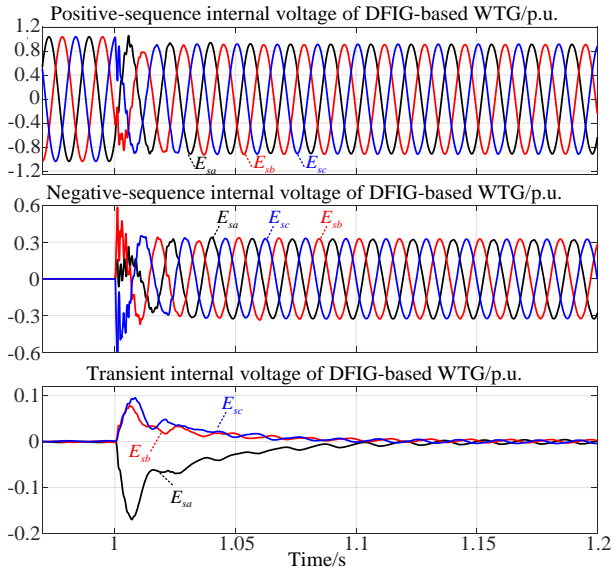


Fig. 12. Positive-sequence, negative-sequence and transient internal voltage of DFIG-based WTG when $K_V=0$.

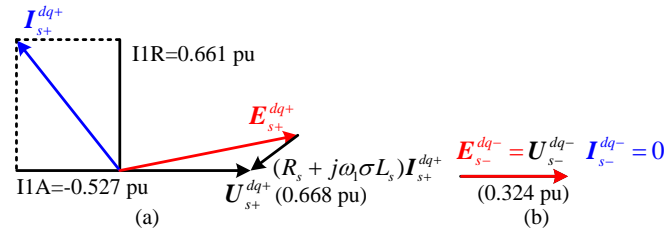


Fig. 13. Spatial diagram of the vectors of the DFIG equivalent circuit when $K_V=0$: (a) positive-sequence vectors; (b) negative-sequence vectors.

It can be seen that the magnitudes of the positive- and negative-sequence internal voltage vectors quickly reach their steady-state values within 30ms, which is much faster than the sub-transient and transient time constants of the SG. It is because, with the inner-loop control, the time constant of the rotor flux linkage branch is changed from τ_r to τ_{ri} . Moreover, the transient internal voltage vector gradually decay to zero to mimic the inductance in (34).

The spatial diagram of positive- and negative-sequence vectors of stator variables in the steady state is shown in Fig. 13. It indicates that, when the K_V is set to 0, DFIG-based WTG has to generate a negative-sequence internal voltage equal to the negative-sequence stator voltage to eliminate the negative-sequence stator current. On the other hand, the current capacity of RSC is all reserved to the I1R and I1A injections.

The internal voltage of the DFIG-based WTG is also shown

for $K_V = 2$ in Fig. 14, and its components are shown in Fig. 15. It can be seen that the magnitude of the negative-sequence internal voltage is reduced by the I2R injection. It makes use of the negative-sequence voltage drop to provide the required I2R as shown in the spatial diagram in Fig. 16 (b). Moreover, it is noted that the positive-sequence internal voltage and stator current in Fig. 16 (a) differ from those in Fig. 13 (a), because the current capacity is first assigned to I2R injection. It highlights the coupling between positive- and negative-sequence internal voltage vectors mentioned in Section IV.B.

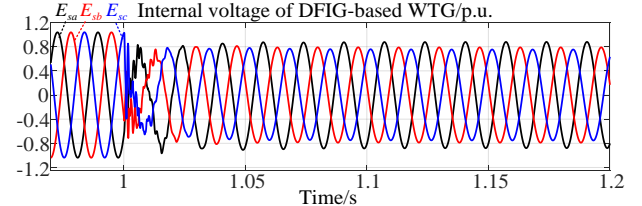


Fig. 14. Three-phase internal voltage of DFIG-based WTG when $K_V=2$.

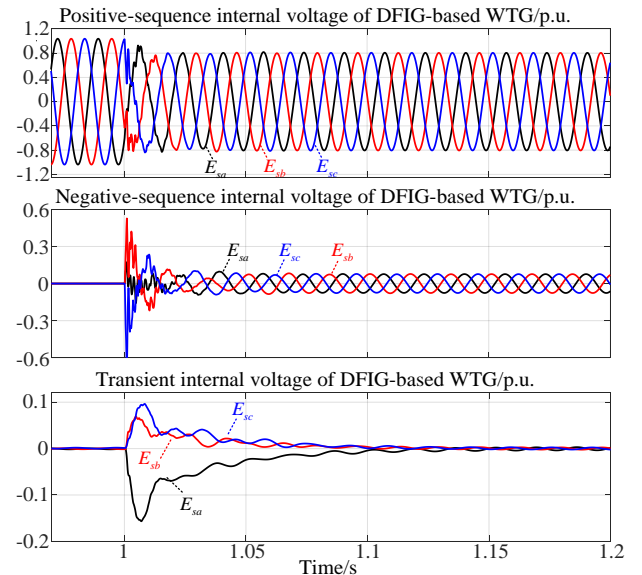


Fig. 15. Positive-sequence, negative-sequence and transient internal voltage of DFIG-based WTG when $K_V=2$.

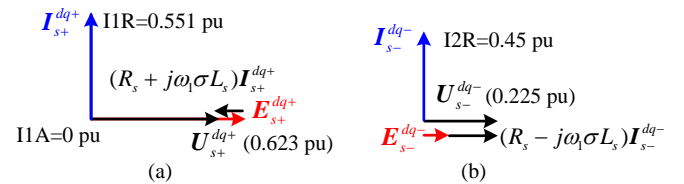


Fig. 16. Spatial diagram of the vectors of the DFIG equivalent circuit when $K_V=2$: (a) positive-sequence vectors; (b) negative-sequence vectors.

V. CONCLUSION

During asymmetrical faults, DFIG-based WTGs are controlled with schemes designed to meet different objectives for the positive-sequence, negative-sequence, and transient components. These AFRT control schemes complicate the fault signatures. This paper proposes a new approach to define both the internal voltage vectors and the equivalent circuit of DFIG-based WTGs, similar to the conventional approach in the modeling of SGs. The responses of the internal voltage vectors and the underlying determinants are presented through comparisons with SGs. The main conclusions are:

(1) During asymmetrical faults, only a positive-sequence internal voltage vector is induced in the SG. Due to the DC excitation, the magnitude of the internal voltage gradually decays with the time constants of the damper and field windings in the sub-transient and transient periods, while the angle and frequency are physically determined by the rotor position and speed. In contrast, due to the flexibility of AC excitation of the DFIG, positive-sequence, negative-sequence and transient internal voltage vectors are induced, and their characteristics are shaped by the corresponding control schemes.

(2) With the inner-loop control, the response time of the positive- and negative-sequence internal voltage vectors of the DFIG-based WTG is effectively reduced from the inherent time constant to the one dominated by the control parameters. Both the magnitude and phase angle rapidly reach their steady-state values for providing the required I2R, I1R and I1A. Due to the voltage and current limits of the RSC, the positive- and negative-sequence internal voltage vectors are coupled. The positive-sequence internal voltage can also be altered by changing the I2R injection factor.

(3) During faults, rotor flux linkage cannot be altered abruptly and thus a transient internal voltage vector is induced in the DFIG. When control schemes are employed to speed up the decay of these transient components, the transient internal voltage vector of DFIG mimics an inductance.

This paper provides key points in explaining the behavior of DFIG-based WTGs for protection coordination studies and control system design.

VI. REFERENCES

- [1] A. K. Elnaggar, J. L. Rueda and I. Erlich, "Comparison of short-circuit current contribution of Doubly-Fed induction generator-based wind turbines and synchronous generator," *IEEE Grenoble Conf.*, 2013.
- [2] "Fault current contributions from wind plants," *68th Annual Conf. for Protective Relay Engineers*, College Station, TX, 2015, pp. 137-227.
- [3] Y. Chang, M. Zhao and I. Kocar, "The Impact of DFIG Control Schemes on Negative-Sequence based Differential Protection Elements," *Electric Power Systems Research*, vol. 211, no. 108564, Oct. 2022.
- [4] "Impact of Inverter-Based Resources on Protection Schemes Based on Negative Sequence Components". Palo Alto, CA: EPRI, 2019.
- [5] "Impact of Renewables on System Protection: Wind/PV Short-Circuit Phasor Model Library and Guidelines for System Protection Studies". Palo Alto, CA: EPRI, 2016.
- [6] Z. He, M. Lu, L. Hang, P. Zeng and Y. Liu, "Capacitor voltage imbalance mechanism and balancing control of MMC when riding through PTG fault," *CSEE Journal of Power and Energy Systems*, Early Access, 2022.
- [7] Y. Chang; J. Hu, G. Song; X. Kong, Y. Yuan, "Impact of DFIG-based wind turbine's fault current on distance relay during symmetrical faults," *IET Renew. Power Gener.*, vol. 14, no. 16, pp. 3097-3102, Dec 2020.
- [8] Y. Chang, I. Kocar, E. Farantatos, A. Haddadi and M. Patel, "Short-Circuit Modeling of DFIG-based WTG in Sequence Domain Considering Various Fault-Ride-Through Requirements and Solutions," in *IEEE Transactions on Power Delivery*. doi: 10.1109/TPWRD.2023.3235985
- [9] R. Gagnon, M. Fecteau, P. Prud'Homme, E. Lemieux, G. Turmel, D. Pare and F. Duong, "Hydro-Québec Strategy to Evaluate Electrical Transients Following Wind Power Plant Integration in the Gaspésie Transmission System," *IEEE Trans. Sustain. Energy*, vol. 3, pp. 880-889, Oct. 2012.
- [10] G. Li, B. Zhang, J. Wang, Z. Bo, T. Yip, D. Writer and Y. Lei, "DFIG-based wind farm electromagnetic dynamic model and impact on protection relay of transmission network," *Int. Conf. on Advanced Power System Automation and Protection*, Beijing, 2011, pp. 694-698.
- [11] U. Karaagac, H. Saad, J. Peralta, and J. Mahseredjian, "Doubly-fed induction generator based wind park models in EMTP-RV," Polytech. Montreal, Internal rep., Apr. 2016.
- [12] R. A. Walling, E. Gursoy and B. English, "Current contributions from Type 3 and Type 4 wind turbine generators during faults," *PES T&D*, Orlando, FL, 2012, pp. 1-6.
- [13] Y. Chang, I. Kocar, J. Mahseredjian and U. Karaagac, "Analytical Characterization of DFIG Response to Asymmetrical Voltage Dips for Efficient Design," *Electric Power Systems Research*, vol. 211, no. 108553, pp. 1-7, Oct. 2022.
- [14] S. Yang, T. Zhou, L. Chang, Z. Xie and X. Zhang, "Analytical Method for DFIG Transients During Voltage Dips," *IEEE Trans. Power Electron.*, vol. 32, no. 9, pp. 6863-6881, Sept. 2017.
- [15] G. Pannell, D. J. Atkinson and B. Zahawi, "Analytical Study of Grid-Fault Response of Wind Turbine Doubly Fed Induction Generator," *IEEE Trans. Energy Convers.*, vol. 25, no. 4, pp. 1081-1091, Dec. 2010.
- [16] Y. Chang, J. Hu, W. Tang and G. Song, "Fault Current Analysis of Type-3 WTs Considering Sequential Switching of Internal Control and Protection Circuits in Multi Time Scales during LVRT," *IEEE Transactions on Power Systems*, vol. 33, no. 6, pp. 6894-6903, Nov. 2018.
- [17] Y. Chang, J. Hu and X. Yuan, "Mechanism Analysis of DFIG-based Wind Turbine's Fault Current during LVRT with Equivalent Inductances," *IEEE Journal of Emerging and Selected Topics in Power Electronics*, vol. 8, no. 2, pp. 1515-1527, June 2020.
- [18] A. El-Naggar and I. Erlich, "Fault Current Contribution Analysis of Doubly Fed Induction Generator-Based Wind Turbines," *IEEE Trans. Energy Convers.*, vol. 30, no. 3, pp. 874-882, Sept. 2015.
- [19] T. Kauffmann, U. Karaagac, I. Kocar, S. Jensen, J. Mahseredjian and E. Farantatos, "An Accurate Type III Wind Turbine Generator Short Circuit Model for Protection Applications," *IEEE Trans. Power Del.*, vol. 32, no. 6, pp. 2370-2379, Dec. 2017.
- [20] D. F. Howard, J. Liang and R. G. Harley, "Short-Circuit Modeling of DFIGs With Uninterrupted Control," *IEEE Journal of Emerging and Selected Topics in Power Electronics*, vol. 2, no. 1, pp. 47-57, March 2014.
- [21] P. Kundur, "Synchronous Machine Representation in Stability Studies," in *Power System Stability and Control*, McGraw-Hill, 1993, pp.184-191.
- [22] B. R. Prentice, "Fundamental Concepts of Synchronous Machine Reactances," *Transactions of the American Institute of Electrical Engineers*, vol. 56, no. 12, pp. 1-21, Dec. 1937.
- [23] P. M. Anderson, "System Characteristics," in *Power System Protection*, 1, Wiley-IEEE Press, 1999, pp.147-194.
- [24] J. Pyrhonen, V. Hrabovcová, and S. R. Semken, "Fundamentals of space-vector theory," in *Electrical Machine Drives Control: An Introduction: An Introduction*, 1, Chichester, West Sussex, United Kingdom: Wiley-IEEE Press, 2016, pp.66-90.
- [25] Math H. Bollen, "Voltage sags-characterization," in *Understanding Power Quality Problems: Voltage Sags and Interruptions*, 1, Wiley-IEEE Press, 2000, pp.139-251.
- [26] G. Abad, J. Lopez, M. A. Rodriguez, L. Marroyo, and G. Iwanski, "Analysis of the DFIM Under Voltage Dips," in *Doubly Fed Induction Machine: Modeling and Control for Wind Energy Generation Applications*, 1, Wiley-IEEE Press, 2011, pp.265-301.
- [27] Y. Chang, I. Kocar, J. Hu, U. Karaagac, K. W. Chan and J. Mahseredjian, "Coordinated Control of DFIG Converters to Comply with Reactive Current Requirements in Emerging Grid Codes," *Journal of Modern Power Systems and Clean Energy*, vol. PP, no. 99, pp. 1-12, Oct. 2021.
- [28] L. Harnefors, M. Bongiorno and S. Lundberg, "Input-Admittance Calculation and Shaping for Controlled Voltage-Source Converters," *IEEE Trans. Ind. Electron.*, vol. 54, no. 6, pp. 3323-3334.
- [29] Y. Chang and J. Hu, "Modeling, analysis and parameters design of rotor current control in DFIG-based wind turbines for dynamic performance optimizing," *2017 IEEE Energy Conversion Congress and Exposition (ECCE)*, Cincinnati, OH, 2017, pp. 3303-3308.
- [30] VDE: "VDE-AR-N 4120: Technical requirements for the connection and operation of customer installations to the high-voltage network (TCC high-voltage)," 2015.
- [31] D. Xiang, L. Ran, P. J. Tavner and S. Yang, "Control of a doubly fed induction generator in a wind turbine during grid fault ride-through," *IEEE Trans. Energy Convers.*, vol. 21, pp. 652-662, Sept. 2006.
- [32] D. Zhu, X. Zou, L. Deng, Q. Huang, S. Zhou and Y. Kang, "Inductance-Emulating Control for DFIG-Based Wind Turbine to Ride-Through Grid Faults," *IEEE Trans. Power Electron.*, vol. 32, no. 11, pp. 8514-8525, Nov. 2017.
- [33] C. Concordia, *Synchronous Machines Theory and Performance*, vol. I. New York: Wiley, 1951, p. 54.